

First observation of a plasmon-mediated tunable photoresponse in a grating-gated InGaAs/InP HEMT for millimeter-wave detection

Nima Nader Esfahani^{*a,b,c}, Robert. E. Peale^a, Walter R. Buchwald^b,
Joshua R. Hendrickson^c and Justin W. Cleary^c

^aDepartment of Physics, University of Central Florida, Orlando FL, USA 32816

^bSolid State Scientific Corporation, Nashua, NH 03060

^cAir Force Research Laboratory, Sensors Directorate, Wright Patterson AFB OH 45433

ABSTRACT

A tunable resonant photoresponse to millimeter-waves is demonstrated in a grating-gated high electron mobility transistor (HEMT) formed by an InGaAs/InP heterostructure. The gate consists of a metal grating with 9 μm period, which was designed to couple mm-radiation to plasmons in the two-dimensional electron gas (2DEG) of the HEMT. The resonant excitation of plasmons, which shifts with gate-bias, changes the channel conductance. These devices have potential as chip-scale frequency-agile mm-wave detectors, which may be scaled to THz frequencies.

Keywords: HEMT, Plasmon, terahertz, 2DEG

1. INTRODUCTION

Recent investigations of chip-scale, mm-wave and terahertz radiation detectors [1-4] have emphasized high-speed tunable resonant excitations of plasmons in a two-dimensional electron gas (2DEG). Such 2DEGs occur at the interface of two semiconductors with a conduction band discontinuity. Coupling structures such as gratings [2-6] or antennae [1] are required to compensate for the inherent momentum mismatch occurring between the incident radiation and excited plasmon mode. The excitation of plasmons results in significant absorption of the incident electromagnetic wave as has been observed by transmission spectroscopy in Si [5], InP [6], and GaN [7] materials systems. In some cases, this excitation gives rise to a change in channel conductance [1-4]. In the device investigated here, the grating also doubles as a gate, which allows for the tuning of the plasmon absorption frequency because of the dependence of the plasmon dispersion relation on sheet charge density. A tunable electrical photoresponse provides a basis for potential on-chip THz and mm-wave spectral detection.

In general, the momentum matching grating period is much smaller than the incident wavelength, which results in the grating becoming polarized at the photon frequency. This polarization induces localized alternating fields with the grating spatial periodicity. These local fields penetrate the underlying semiconductor layers and perturb the 2DEG. The characteristic length scale of the grating structure defines the optical frequencies of the excited plasmons via their dispersion relation, and in consequence defines possible resonant changes in channel conductance. The plasmon dispersion relation is a function of both material and structure. The InGaAs/InP materials system has been selected in part because of the possibility of sharp THz plasmon resonances at high frequencies due to high sheet charge density, large mobility and low electron effective mass, which in principle allow narrow resonances at THz frequencies.

This work presents our first observation of an *electrical* photo-response due to plasmon excitation in the 2DEG of an InGaAs/InP HEMT. For experimental convenience, due to the availability of stable and highly functional mm-wave sources, this first demonstration has been performed at millimeter wavelengths.

2. THEORETICAL CONSIDERATIONS

The dispersion relation for two-dimensional plasmons is [5]

$$\omega_n^2 = \frac{e^2 n_s q_n}{m^* \epsilon_0} (\epsilon_b + \epsilon_t \coth(q_n d))^{-1}, \quad (1)$$

where ω_n is the frequency of the n^{th} integer order plasmon, e the electron's charge, m^* the effective mass, d the 2DEG depth from the grating, and n_s the 2DEG sheet charge density, The allowed plasmon wavevector q_n takes discrete values $2\pi n/a$ determined by the grating period a . The relative permittivity of the semiconductor layers on top and beneath the 2DEG are denoted by ϵ_t and ϵ_b , respectively.

The transmittance spectrum of the device is calculated following the method described in [6, 8]. This method accounts for both perpendicular and parallel polarizations relative to grating strips, although only perpendicular polarization is predicted to contribute to the excitation of plasmons inside 2DEG. These calculations require knowledge of n_s and the relaxation time τ of the 2DEG. Both quantities are determined via Source-Drain I-V measurements with varying gate bias as described in [6, 9].

The experimental response is interpreted in terms of the calculated transmittance spectrum as follows. Synchronous lock-in amplification of the HEMT Source-Drain current I_{SD} , via the voltage drop V_L across a load resistor R_L , with mm-wave frequency modulation of Δf , gives a lock-in output [9]

$$V_{out}(V_g, f) = \frac{2}{\pi} \left(\frac{10V}{V_{range}} \right) \left(\frac{dV_L(v_g, f)}{df} \right) \Delta f . \quad (2)$$

In Eq. 2, V_{range} is the selected sensitivity of the lock-in amplifier. Since the high-impedance lock-in input draws approximately no current, Eq. 2 may be expressed in terms of I_{SD} as

$$V_{out}(V_g, f) = \frac{2}{\pi} \left(\frac{10V}{V_{range}} \right) \left(\frac{dI_{SD}(v_g, f)}{df} \right) R_L \Delta f . \quad (3)$$

The change dI_{SD} may be written as $d(BWA)$, where B is an unknown coupling factor between plasmonic absorption and the change in channel conductance, W is the effective radiation power transferred to the 2DEG at each frequency, and A is absorbance. Using $A = I-R-T$ for absorbance, where T is the transmittance and R the constant front surface reflectance, gives

$$V_{out}(V_g, f) = \frac{2}{\pi} \left(\frac{10V}{V_{range}} \right) \left\{ \frac{-[(dBWT)]}{df} \right\} R_L \Delta f . \quad (4)$$

B is assumed to be frequency and gate-bias independent for simplicity. The microwave power inside the waveguide is independent of frequency due to power leveling, but once it leaves the waveguide and is incident on the sample, the value of W may vary strongly with wavelength due to interference effects. However, it is assumed that W is constant over the small Δf utilized so that there will be no artifacts due to amplitude modulation. The lock-in output is then

$$V_{out}(V_g, f) = \frac{2}{\pi} \left(\frac{10V}{V_{range}} \right) BW \left(\frac{-dT(v_g, f)}{df} \right) R_L \Delta f . \quad (5)$$

3. EXPERIMENTAL DETAILS

The InGaAs/InP HEMT was commercially grown by molecular beam epitaxy. The specified layered structure of the HEMT material is presented in figure 1. The doped-InGaAs cap layer was etched away and a 20 nm Ti layer was deposited in the gate region. The Ti thickness is significantly less than the estimated skin depth of ~1 micron at 100 GHz to allow transmission. Grating stripes of 9 μm period and 22% duty cycle were fabricated by standard e-beam lithography with heights of 150nm, (15 nm Ti/100 nm Au). Source, Gate, and Drain contact pads were fabricated by conventional photolithography with thicknesses of 50 nm Ti/250 nm Au.

75° A InGaAs Cap Si-doped $6 \times 10^{18} \text{ cm}^{-3}$
350° A InAlAs Undoped
δ -doped layer $4 \times 10^{12} \text{ cm}^{-2}$
30° A InAlAs Spacer Undoped
200° A InGaAs Channel Undoped
30° A InAlAs Undoped
δ -doped layer $4 \times 10^{12} \text{ cm}^{-2}$
3000° A InAlAs undoped
InP Substrate

Fig. 1. Commercial HEMT wafer epilayer structure.

The device was fixed to a cold finger inside a Janis SHI-4 closed cycle cryostat. A silicon diode temperature sensor, thermally contacted to the cold finger below the device, was connected to a temperature controller and utilized in a feedback loop to maintain a temperature of approximately 4 K during experiments.

The schematic of the experimental setup is shown in figure 2 (right) while figure 2 (left) presents a cartoon of the horn positioned above the HEMT and oriented for perpendicular polarization. For frequency modulation, a 100 Hz sine wave, with DC offset from 0.7 to 3.0 V, was divided into two paths. One path was high-pass filtered to strip the DC component and amplified for the Lock-in reference. The other path was directly applied to the external Sweep input of a Siemens backward wave oscillator (BWO) to externally sweep and modulate the mm-wave frequency. The DC component set the central frequency of the BWO radiation anywhere between 78 to 103 GHz while the sine wave component modulated the BWO frequency by 100 MHz (+0.1% of the central frequency). A crystal detector was connected via a 10 db directional coupler to monitor the total radiation power. The crystal output was connected to the power leveling circuit of the BWO.

The mm-waves generated by the BWO head are directed toward the cryostat using waveguides and a polarization-preserving horn. A polyethylene vacuum window allowed the radiation to pass into the cryostat and irradiate the device. The head could be rotated about the optical axis to study polarizations effects with respect to the device gratings. During measurements, a constant voltage of 0.5 V was applied to the Source with the Drain connected to ground via a 100 Ω load resistor. Gate biases V_g of 0, -0.1 and -0.2 V were applied with respect to Drain.

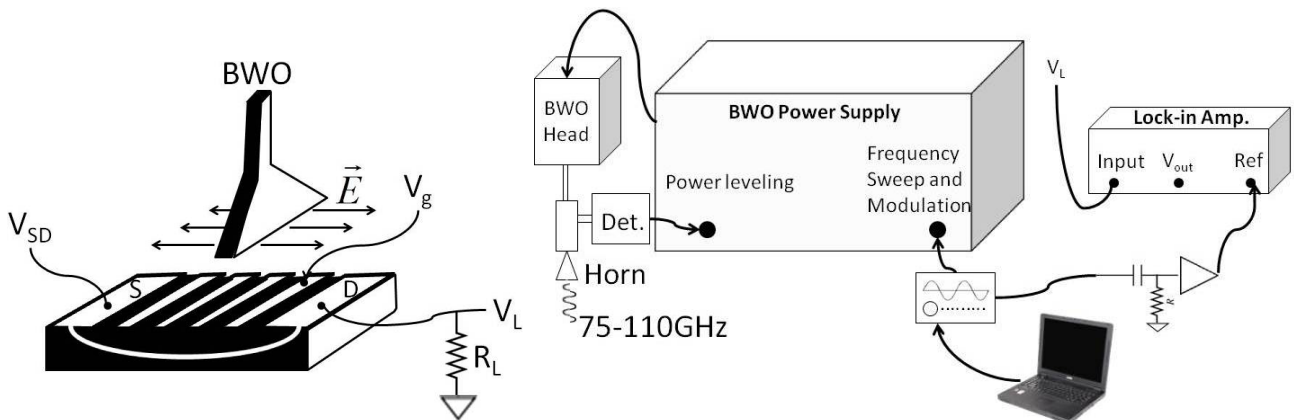


Fig. 2. (Left) Drawing of the horn on top of the grating-gated HEMT with radiation polarized perpendicular to the grating (Right) Schematic of the experimental setup

4. RESULTS

Source-Drain IV-measurements were completed as a function of gate-bias in order to determine n_s and τ of the device. Data taken at the temperature of 4 K for V_g between 0 and -0.5 V with resolution of -0.1 V are presented in figure 3. Source-Drain current, I_{SD} , saturates at V_s in the range of 1 to 1.5 V to different levels which decrease with increasing negative gate bias until the HEMT reaches pinch off at around $V_g = -0.6$ V. The three connected solid symbols indicate three bias points used during photoresponse measurements, which were all performed below saturation conditions. Following [9], the saturation current values at each V_g allows us to determine the relaxation time to be 0.37 ps, and the sheet charge density, n_s , to be 1.39, 1.21 and $1.04 \times 10^{12} \text{ cm}^{-2}$ at gate biases of 0, -0.1 and -0.2 V.

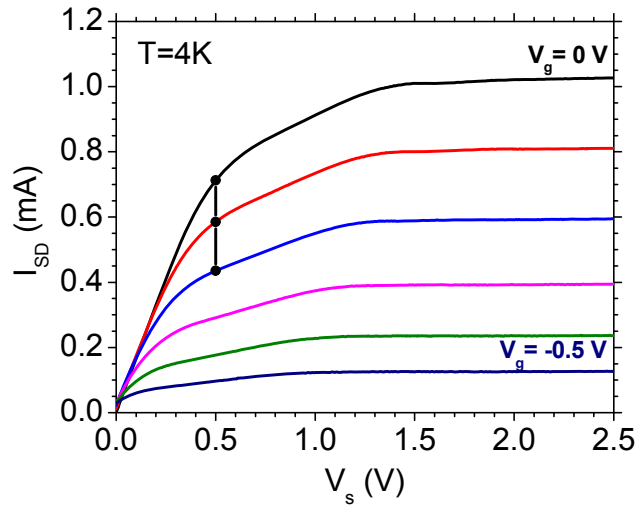


Fig. 3. Measured Source-Drain Current as a function of applied source voltage at $T = 4$ K. The extremes of the gate bias are shown next to their corresponding curves with the resolution of V_g being -0.1 V.

Figure 4 (top) presents the calculated device transmittance spectrum at 4 K as a function of V_g for frequencies up to 500 GHz. The figure pictorially represents approximately the low frequency half of the resonance since the plasmon resonances tend to be very broad in the mm-wave region. Peak absorption occurs at 365, 340 and 320 GHz for $V_g = 0, -0.1$ and -0.2 V, respectively, as indicated by symbols. This shows a redshift with increasing negative V_g and thus decreasing n_s which is in agreement with Eq. 1. The absorption band also becomes shallower, which is reasonable since electrons are required for plasmon absorption and increasing the negative gate-bias results in the reduction of the 2DEG free carrier concentration.

Figure 4 (bottom) presents the slope of the transmission with respect to frequency (dT/df) of the same curves presented in Figure 4 (top). During the photoresponse measurements, the lock-in output is proportional to the slope of the transmission spectrum, Eq. 5, therefore, these curves will be utilized in comparisons to experiment. The horizontal bar indicates the tuning range of the BWO, which falls near the low-frequency side of the resonance with a significant dT/df . Minima of plasmonic absorption lines are marked by symbols with colors.

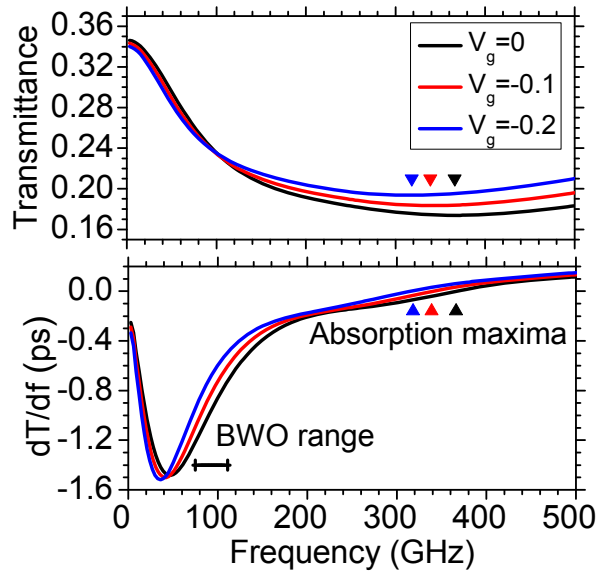


Fig. 4. (Top) Calculated transmittance spectra in the range of 0-500 GHz. Absorption maxima for three different gate biases are marked with symbols. **(Bottom)** Calculated dT/df spectra in the same frequency range. The horizontal bar indicates our BWO range.

Figure 5 presents the photoresponse of the device (lock-in output as shown in Fig. 2) to mm-waves in the frequency range of 78 to 103 GHz for the gate bias of 0, -0.1 and -0.2 V. Also shown in figure 5 are linear fits to the measured data. The detected photoresponse shows sharp features at discrete frequencies as opposed to a continuous electrical response. This can be attributed to interference of incident mm-waves and the formation of standing waves. When standing wave nodes occur at the grating, no power is transferred to the plasmons and no electrical response will be detected. Oppositely, at frequencies in which anti-nodes occur at the grating, coupling to plasmons and corresponding electrical response may occur.

During the measurements, the gain horn was oriented to produce an incident electric field perpendicular as shown in Fig. 2 (left), or parallel. No plasmon excitation was expected at the parallel polarization because it cannot polarize the grating stripes, however, the observed effects in Fig. 5 are similar for both polarization cases. This suggests that the polarization of the mm-waves reaching the 2DEG is not the simple polarization cases expected by the experimental setup. Comparison of the plots in Fig. 5 reveals another feature. At frequencies where the HEMT demonstrates a relatively strong photoresponse for the radiation with nominal perpendicular polarization, a weak response can be observed in the opposite polarization, and vice-versa. This suggests that rotating the polarization converts standing wave nodes to anti-nodes and vice-versa. How this occurs, remains unclear and the overall polarization and related effects will be the focus of further investigations.

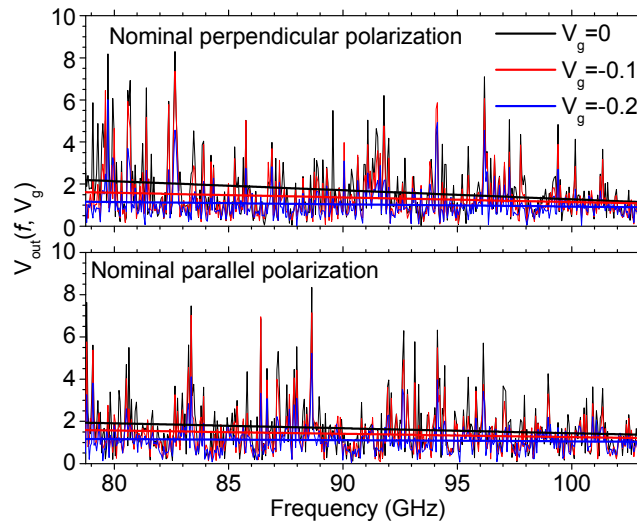


Fig. 5. Photoresponse of the HEMT at $T = 4$ K to mm-wave radiations for two nominal polarizations and three gate biases. Straight lines are linear fits that represent an average over the standing wave effects. The indicated polarizations were the nominal polarizations expected from the horn.

In Fig. 5, the plotted linear fits represent an average over the photoresponse fluctuations caused by standing waves. Figure 6 (left and right) compares these lines to the theoretical expectations from Fig. 4. Both experimental polarizations are compared with theory since the actual polarizations were not clear and each nominal polarization case likely has contributions from perpendicular and parallel components. In Fig. 6 the data fits are vertically scaled to the analytical calculated values at the center frequency of the plots. In all cases, the response decreases with increasing frequency and with increasing negative gate bias. However, the slopes of the experimental data fits differ from that of the calculated curves. The calculated lines in both plots are relatively parallel to each other, while the experimental curves converge at higher frequencies. The slopes agree better if the data is compared to a higher frequency range in the calculated curves (~ 141 - 166 GHz). This indicates that the measured plasmon activity may be occurring at lower frequencies, by approximately 68 GHz, than predicted by theory. This may occur if the n_s and/or τ values have been over estimated. Similar discrepancies between experimental measurements and theory have precedent [6] and have been the cause of considerable speculation [11-13].

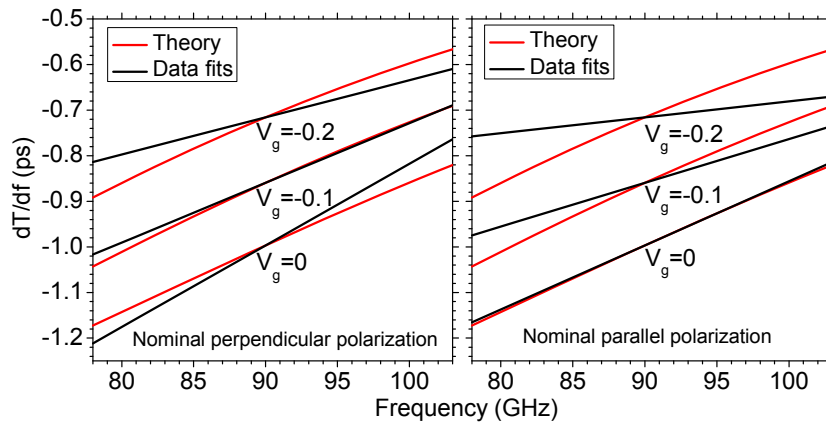


Fig. 6. data fits with nominal perpendicular polarization (**Left**) and parallel polarization (**Right**) to the grating strips compared with theory. Gate biases are labeled beside each of the groups of lines.

5. SUMMARY AND OUTLOOK

An electrical photoresponse, that can be attributed to tunable resonant absorption of mm-waves by 2D-plasmons in the channel of a HEMT, has been observed for the first time in the InGaAs/InP materials system. Experimental observations agree with theory in two major ways supporting the interpretation of resonant absorption due to plasmon excitation. Namely, the measured response decreases with increasing frequency and with increasing applied negative gate bias as predicted and, the observed decrease of the photoresponse effect, as a function of increasing negative gate bias, can be attributed to the depletion of charge in the channel of the device as expected. The lack of strong polarization dependence and a mismatch between the transmission rate of change with frequency for the expected and observed effects remain to be resolved and will be the focus of further investigations.

6. ACKNOWLEDGMENTS

NNE and JWC would like to acknowledge support from the Air Force Office of Scientific Research (Program Manager Dr. Gernot Pomrenke) under LRIR number 12RY10COR. REP acknowledges support by the Air Force office of Scientific Research (Program Manager Dr. Gernot Pomrenke) under grant number FA95501010030. JRH would also like to acknowledge support from the Air Force Office of Scientific Research (Program Manager Dr. Gernot Pomrenke) under LRIR number 10RY04COR.

REFERENCES

- [1] G. C. Dyer, S. Preu, G. R. Azin, J. Mikalopas, et al., "Enhanced performance of sub-terahertz detection in a plasmonic cavity", *Appl. Phys. Lett.* **100**, 083506 (2012)
- [2] E. A. Shaner, M. Lee, M. C. Wanke, A. D. Grine, J. L. Reno and S. J. Allen, "Single-quantum-well grating-gated terahertz plasmon detectors.", *Appl. Phys. Lett.* **87**, 193507 (2005)
- [3] X. G. Peralta, S. J. Allen, M. C. Wanke, N. E. Harff, J. A. Simmon, et al., "Terahertz photoconductivity and plasmon modes in double-quantum-well field-effect transistors", *Appl. Phys. Lett.* **81**, 1627-1629 (2002)
- [4] W. Knap, Y. Deng, S. Rumyantsev, M. S. Shur, "Resonant detection of subterahertz and terahertz radiation by plasma waves in submicron field-effect transistors", *Appl. Phys. Lett.* **81**, 4637-4639 (2002)
- [5] S. J. Allen, Jr., D. C. Tsui, and R. A. Logan, "Observation of the Two-Dimensional Plasmon in Silicon Inversion Layers", *Phys. Rev. Lett.* **38**, 980 (1977).
- [6] H. Saxena, R. E. Peale and W. R. Buchwald, "Tunable two-dimensional Plasmon resonances in an InGaAs/InP HEMT", *J. Appl. Phys.* **105**, 113101 (2009).
- [7] Muravjov, A. V., Veksler, D. B., Popov, V. V., Polischuk, O. V., Pala, N., Hu, X., Gaska, R., Saxena, H., Peale, R. E., and Shur, M. S., "Temperature dependence of plasmonic terahertz absorption in grating-gate gallium-nitride transistor structures," *Appl. Phys. Lett.* **96**, 042105 (2010).
- [8] L. Zheng, W. L. Schaich, and A. H. MacDonald, "Theory of two-dimensional grating couplers, *Phys. Rev. B* **41**, 8493 (1990).
- [9] A. A. Grindberg and M. Shur, "A new analytical model for heterostructure field-effect transistors", *Jour. Appl. Phys.* **65**, 2116 (1989)
- [10] Dunlop, R. A., [Experimental Physics], Oxford University Press, Oxford, New York and Toronto, 102-107 (1988).
- [11] R. E. Peale, H. Saxena, W. R. Buchwald, G. Aizin, A. V. Muravjov, D. B. Veksler, N. Pala, X. Hu, R. Gaska, M. S. Shur, "Grating-gate tunable plasmon absorption in InP and GaN based HEMTs," *Proc. SPIE* 7467-25 (2009).
- [12] J. W. Cleary, R. E. Peale, H. Saxena, and W. R. Buchwald, "Investigation of plasmonic resonances in the two-dimensional electron gas of an InGaAs/InP high electron mobility transistor," *Proc. SPIE* 8023, 80230X (2011)
- [13] N. Nader Esfahani, J. W. Cleary, R. E. Peale, W. R. Buchwald, C. J. Fredricksen, J. R. Hendrickson, M. S. Lodge, B. D. Dawson and M. Ishigami, "InP- and Graphene-based grating-gated transistors for tunable THz and mm-wave detection.", *Proc. SPIE* 7373-80 (2012).